Characterization of Spinel Lithium Manganite Prepared by Citrate Sol-Gel Method

Young-Sik Hong, Hyu-Bum Park, Ji-Eun Yi†, Chi-Hwan Han, and Si-Joong Kim*

Department of Chemistry, Korea University, Seoul 136-701, Korea
†Korea Basic Science Institute, Seoul 136-701, Korea
Received April 2, 1997

The powder characteristics of $LiMn_2O_4$ prepared by the citrate sol-gel method have been investigated. The optimum pH for the preparation of homogeneous citrate gel was calculated by the theoretical consideration of thermodynamic equilibrium constants for metal-citrate complexes and metal salts. The obtained citrate gel was prefired at 300 °C and calcined at 300-700 °C for 1 h. The obtained powders were characterized by TG/DSC, FT-IR spectrometer, X-ray diffractometer, SQUID magnetometer, SEM, and particle size analyzer. It was observed that the mixed phases of spinel $LiMn_2O_4$ and Mn_3O_4 were transformed into spinel $LiMn_2O_4$ phase and the vibrational bands due to the carbonate and nitrate were also disappeared over 400 °C. At temperatures below 150 K, inverse molar susceptibilities of every sample began to show an antiferromagnetic ordering of Mn magnetic moments.

Introduction

Among the various cathode materials, the spinel $Li_xMn_2O_4$ has been widely studied not only because it can be simply prepared by the solid state reaction, but also because it has the advantageous of its high theoretical energy density, low cost, and less toxity, as compared to those of cobalt, nickel or vanadium. However, the conventional solid state reaction method requires long-range diffusion of reactants and may result in inhomogeneous composition, larger particle size, and longer periods of calcination.[1-3] In order to achieve a larger current capacity and reliability of the lithium batteries, therefore, it is necessary to prepare homogeneous fine $LiMn_2O_4$ powders by solution methods.

There have been considerable interests in developing synthetic techniques to maintain a homogeneous reactant distribution at low temperature. Recently, the solution methods by means of complexing or gelling agents, such as glycine-nitrate,[4,5] tetraformal trisazine,[6] carbohydrate,[7] heteronuclear complex[8] and polymers,[9-11] have been devised to synthesize $LaMO_3$ powders (M=Cr, Mn, Fe, and Co) at low temperature. Similarly, some investigators have reported the electrochemical properties of lithium transition metal oxides synthesized by using polymer precursors as gelling agents.[12-14] In the polymer precursor method, the metal ions are surrounded by polymer chains, which suppresses the precipitation of metal salts during the evaporation of solvent.

However, there are only a few solution methods for lithium transition metal oxides using complexing agents. Chang *et al.*[15] have prepared the $Li_xCo_yNi_{1-y}O_2$ powders using the citrate sol-gel method, but a systematic survey for the synthesis of $LiMn_2O_4$ has not given yet. The major problem in this method, as well as other complexing methods, is the low thermodynamic equilibrium constant of lithium complexes.

In this study, we have applied the citrate sol-gel to obtain spinel $LiMn_2O_4$ powders, based on the consideration of the complexing ability of citric acid to form metal-citrate complexes at specified pH.

Theoretical Consideration of the Distribution of Chemical Species

Since the chelating ability of citric acid with metal ions is highly dependent on the pH of the solution, it is required to investigate the behavior of ionic species present in the aqueous solution. In aqueous solutions and at equimolar manganese and citric acid concentrations, citric acid reacts with Mn^{2+} to form two types of monomeric complexes: $MnC_6H_6O_7$ and $MnC_6H_5O_7^-$. Thus, to prepare a homogeneous citrate gel, we have carried out theoretical calculation on the concentration of the chemical species, based on the thermodynamic equilibrium constants as listed in Table 1.[16-19]

Table 1. Thermodynamic equilibrium constants for the possible species in the Li(I)-Mn(II)-citric acid-H_2O system

Equilibria		Equilibrium constants	
H_3L	$= H_2L^- + H^+$	$\log K_1$	3.13
H_2L^-	$= HL^{2-} + H^+$	$\log K_2$	4.76
HL^{2-}	$= L^{3-} + H^+$	$\log K_3$	6.40
H_2O	$= H^+ + OH^-$	$\log K_w$	14
CO_2+H_2O	$= H_2CO_3$	$\log K_1$	−1.46
H_2CO_3	$= HCO_3^- + H^+$	$\log K_2$	−6.35
HCO_3^-	$= CO_3^{2-} + H^+$	$\log K_3$	−10.33
$Mn^{2+} + OH^-$	$= MnOH^+$	$\log\beta_1$	3.4
$Mn^{2+} + 2OH^-$	$= Mn(OH)_2^\circ$	$\log\beta_2$	6.8
$Mn^{2+} + 3OH^-$	$= Mn(OH)_3^-$	$\log\beta_3$	7.0
$Mn^{2+} + 4OH^-$	$= Mn(OH)_4^{2-}$	$\log\beta_4$	7.7
$Mn(OH)_2(s)$	$= Mn^{2+} + 2OH^-$	$\log K_{sp}$	−12.8
$MnCO_3(s)$	$= Mn^{2+} + CO_3^{2-}$	$\log K_{sp}$	−10.4
$Li_3L(s)$	$= 3Li^+ + L^{3-}$	$\log K_{sp}$	2.20
$Li^+ + L^{3-}$	$= LiL^{2-}$	$\log\beta_1$	0.83
$Mn^{2+} + L^{3-}$	$= MnL^-$	$\log\beta_1$	5.5
$Mn^{2+} + HL^{2-}$	$= MnHL$	$\log\beta_2$	9.4

† $\log K_i$: stepwise stability constant; $\log K_{sp}$: solubility product. $\log\beta_i$: overall stability constant.

Figure 1(b) shows the mole fraction of chemical species in the Li-Mn-citric acid-H_2O system with respect to pH, calculated from the solubility diagram (Figure 1(a)). The calculation procedures were reported in detail elsewhere.[17,18,20] Calculations based on stability constants for manganese citrate complexes show that free Mn^{2+}, $MnC_6H_6O_7$, $MnC_6H_5O_7$, and $Mn(OH)_2$(s) are predominant species at pH values of ~3, 4 ~5, 5 ~9, and 9~ in Mn-citric acid-H_2O system, respectively. To avoid the formation of $Mn(OH)_2$ precipitates and obtain the highest amount of citrate complexes, therefore, the optimum pH value can be set as around 7.0. In Li-citric acid-H_2O system, only the two species of Li^+ and $LiC_6H_5O_7^{2-}$ present at all pH ranges and the complete complexation of Li^+ and citric acid does not occur (Figure 1(b)).

Experimental

Preparation. The citrate gel was prepared as follows: at first, lithium nitrate (0.030 mol), manganese nitrate (0.060 mol), and citric acid (0.090 mol) were dissolved with the mole ratio of 1 : 2 : 3 in distilled water. The pH of the mixed solution was adjusted up to 6.5-7 by adding aqueous NH_4OH. The resulting clear solution was heated at 70-75 °C while it was mechanically stirred. After the water evaporated, the solutions turned into a viscous citrate gel with a pale pink in color and amorphous in shape. That is, as the evaporation of solvent is proceeded, the (Li, Mn)-citrate complexes and precipitates did not observed until the amorphous citrate gel was formed.

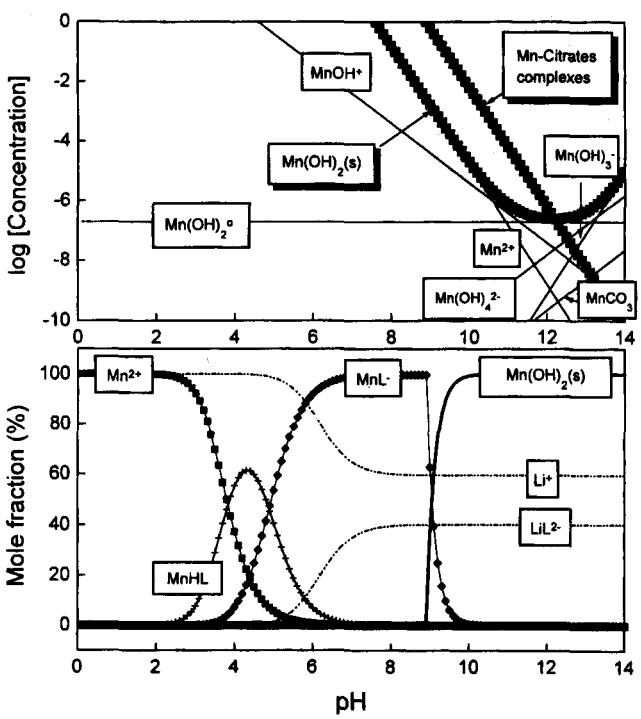

Figure 1. Distribution of (a) hydrolysis products in aqueous solution at equilibrium with a hydroxide solid phase for Mn^{2+} ion (the weighted solid curve is the total concentration of Mn^{2+} in solution) and (b) chemical species in the Li(I)-Mn(II)-citric acid-H_2O system; L^3 =$C_6H_5O_7^3$, HL^2 =$C_6H_6O_7^{2-}$, and H_2L^- =$C_6H_7O_7^-$.

The resulted citrate gel was burnt at 300 °C in air, which is referred as precursor. Once the ignition started at a part of the citrate gel, a flame spontaneously propagated through the bulk of the citrate gel, leaving a voluminous fluffy black powder within 10 min. The precursor was then calcined at 300-700 °C for 1 h in air to obtain a single phase of spinel $LiMn_2O_4$. The calcined powders were referred as LM-calcination temperature.

Instrumentation. The thermal decomposition behavior of the citrate gel was studied using thermogravimeter (TG, Stanton Redcroft TGA-1000) and differential scanning calorimeter (DSC, Stanton Redcroft DSC-1500) with a heating rate of 10 °C/min in air. The phases of precursor and calcined powders were identified by FT-infrared spectrometer (FT-IR, BOMEM MB-102) and X-ray diffractometer (XRD, Rigaku D-MAX III-b) using CuK_α radiation. The crystallite size was calculated from the X-ray line broadening effect using Scherrer's formula, $t=\{t\lambda\}/\{B\cos\theta\}$, where t is crystallite size, k is a shape function (a value of 0.9 was used), λ is the X-ray radiation wavelength, B is the width of the peak at its half maximum, and θ is the angle of incidence. B was determined from the experimental integral width by applying standard correction for the effect of $K_{\alpha1}$-$K_{\alpha2}$ separation and instrumental broadening. The magnetic susceptibility (χ) was determined by using a superconducting quantum interference device (SQUID) magnetometer (Quantum Design, MPMS5) at 4-300 K. The data were measured in a field-cool mode with a magnetic field of H=1 T. The particle size distribution were measured by a laser particle size analyzer (Granulometer HR 850, Cilas-Alcatel). The morphologies of the calcined powders were observed using a scanning electron microscopy (SEM, JEOL JSM 840 A).

Results and Discussion

Preparation of the citrate gel. In the citrate sol-gel method, the equilibrium constant of Li-citrate complex is small and thus the mole fraction of Li-citrate complex is small as shown in Figure 1. It causes a segregation of (Li, Mn)-citrate complexes from uncomplexed Li^+ ions. However, the citrate gel was formed amorphous in shape. Thus the Li^+ and Mn^{2+} ions can be trapped homogeneously on a molecular scale throughout a transparent gel. Such a gel eliminates the problem for inhomogeneity and the need for long-range diffusion during the formation of the spinel $LiMn_2O_4$.

In addition, the citrate sol-gel method has been examined to the synthesis of a $LiNiO_2$, $LiCoO_2$, and $LaMO_3$ (M=Al, Cr, Mn, Fe, Co, and Ni) powders. For (Li, Ni)-, (La, Co)-, and (La, Ni)-citrate gels, precipitates of citrate complexes were formed, whereas the viscous gels were obtained for (Li, Co)-, (La, Al)-, (La, Cr)-, (La, Mn)-, and (La, Fe)-citrate gels. It has not been well understood why the gel formation mechanisms are different from each other.

Thermal behavior of citrate gel. To find a firing condition, TG and DSC analyses were performed as shown in Figure 2(a). The TG curve of the citrate gel in air shows a drastic weight loss at around 250 °C with a small shoulder at 150 °C. The small weight loss below 150 °C accompanied by the two endotherm at 130 and 155 °C in

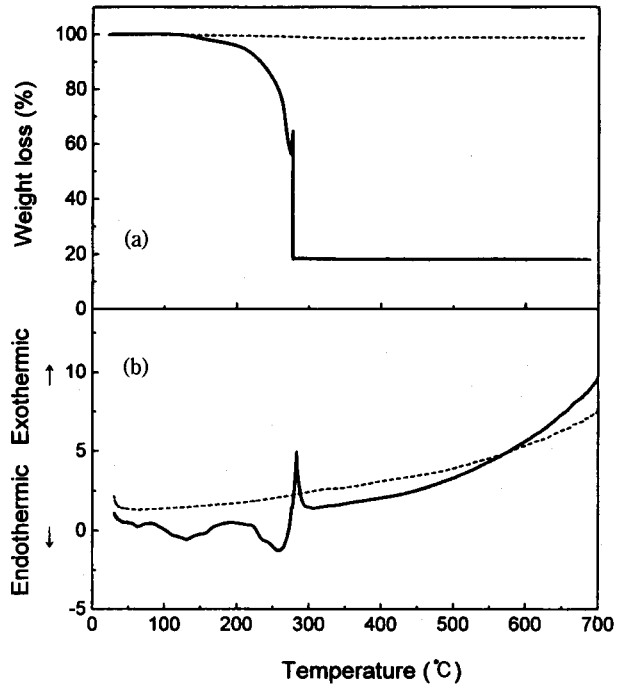

Figure 2. (a) TG and (b) DSC curves of the citrate gel and the precursor with a heating rate of 10 °C/min. (—: citrate gel, —: precursor)

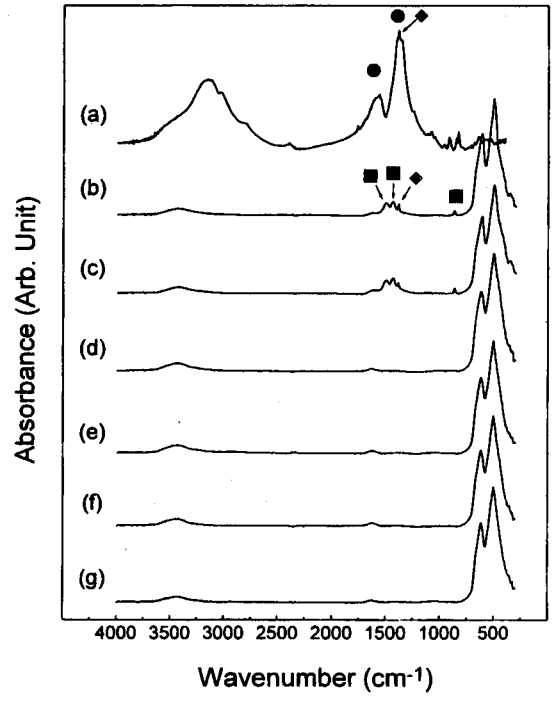

Figure 3. FT-IR spectra of (a) the citrate gel, (b) the precursor, (c) LM-300, (d) LM-400, (e) LM-500, (f) LM-600, and (g) LM-700. (● : carboxylate coordinated to metal, ◈ and ■ : nitrate)

DSC, is ascribed to the evaporation of residual water and the melting of citric acid. The endothermic peak due to the water loss is rather shifted to high temperature because the water is trapped into the highly viscous gel. The abrupt mass decrease above 250 °C might be due to the decomposition of nitrates and citrate complexes.

Since the nitrate ions, acting as an oxidizer, coexist closely with the fuel (citric acid) in a homogeneously mixed state, it can be explosively reacted with the citric acid within a very short period of time. Therefore, the combustion reaction could result in the drastic weight loss due to the rapid decomposition of citric and nitrate ions. And also the bouncing of TG curve at 280 °C results from the explosive decomposition and thus a part of the samples got out of sample container. It was difficult to obtain TG and DSC curves quantitatively in high temperature region. According to TG and DSC analyses of the citrate gel, the minimum firing temperature was found to be above 300 °C to get organic and nitrate-free precursor. The precursor was reexamined to investigate thermal behavior, but no longer weight loss occurs (Figure 2(b)).

FT-IR study of the citrate gel and calcined powders. The complexation of metal ion and citric acid is confirmed by FT-IR spectrum of the citrate gel. Figure 3 shows the FT-IR spectra of the citrate gel, the precursor and the calcined power. The conversion of citric acid into citrate complexes is demonstrated by the replacement of the five characteristic vibrations of -COOH, corresponding to $\nu_{C=O}$= 1740 and 1690 cm^{-1}; δ_{OH}(in-plane)=1420 cm^{-1}, ν_{C-O}=1300-1200 cm^{-1}, and δ_{OH}(out-of-plane)=930 cm^{-1}, by two characteristic vibrations of $-CO_2^-$, corresponding to the antisymmetric and symmetric stretching vibrations near 1580 and 1390 cm^{-1}, respectively. In addition, the sharp band assigned to ν_3 mode of nitrate ion is superimposed to the band of carboxylate groups coordinated to metal.

For the precursor, the bands resulted from the ν_3 and ν_2 vibrational modes of carbonate ions are appeared at 1500 and 1440, and 868 cm^{-1}, respectively.[22] The bands below 750 cm^{-1} were presumably due to metal oxide and ν_4 vibrational modes of carbonate. LM-300 exhibits the same feature with the precursor. The carbonate and the nitrate bands are eliminated by the calcination at 400 °C, whereas two bands at 622 and 512 cm^{-1} assignable to metal-oxygen stretching and oxygen-metal-oxygen deformation modes remain unchanged. It is worthy to note here that the FT-IR spectra after calcining above 400 °C reveal the formation of spinel structure, which is fully consisted with that of $LiMn_2O_4$ reported by Wen *et al.*[22]

XRD study of the calcined powders. Figure 4 shows the XRD patterns for the precursor and the calcined powders. For the precursor and LM-300, the XRD patterns exhibit that the minor phase, such as Mn_3O_4 (JCPDS 24-734, hausmannite) [or γ-Mn_2O_3 (JCPDS 18-803)], coexists with the major phase of $LiMn_2O_4$ (JCPDS 35-782). It is difficult to distinguish between Mn_3O_4 and Mn_2O_3 because the two phases are known to have very similar XRD patterns. For LM-400, XRD analysis indicated the spinel structure with no discernable impurities. With the increase of calcination temperature, there is a gradual increase in the peak intensities accompanied by sharpening of peaks. This may be attributed to the gradual increase in the crystallite size as listed in Table 2.[12] Considering the facts that no crystalline metal carbonates could be observable in the XRD patterns and lithium has much low X-ray scattering power, the carbonate is probably expected to be Li_2CO_3 salts as discussed in FT-IR spectra.

Figure 5 shows the variation of the cubic lattice parameter versus calcination temperature for the calcined powder.

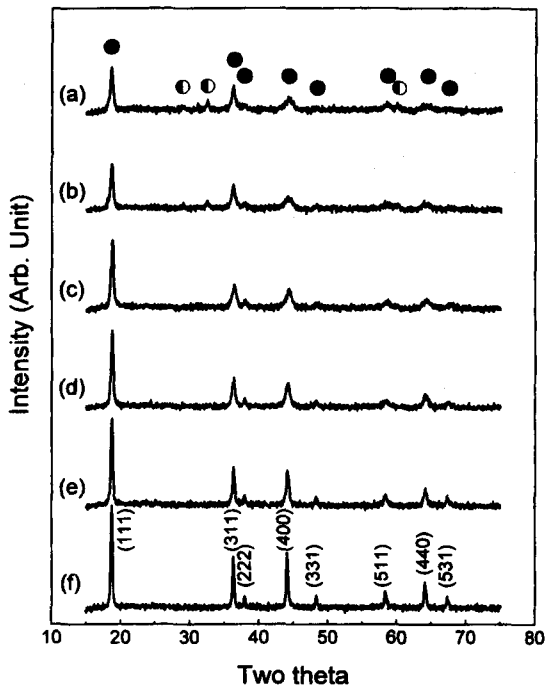

Figure 4. XRD patterns of (a) the precursor (b) the precursor, (c) LM-300, (d) LM-400, (e) LM-500, (f) LM-600, and (g) LM-700. (●: spinel structure, ◐ Mn_3O_4 or Mn_2O_3)

Table 2. Crystallite size, Curie Weiss constant, and mean diameter for the calcined powder

Ccalcination temperature/°C	300	400	500	600	700
primary particle size/nm	50	83	109	173	281
Curie Weiss constnat/K		−107	−123	−151	−214
mean diameter/μm	2.88	2.82	2.90	3.00	3.22

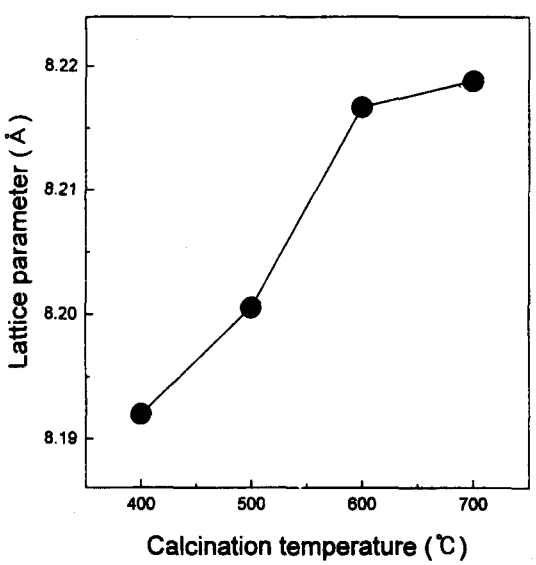

Figure 5. The variation of cubic lattice parameter versus the calcination temperature for the calcined powder.

The lattice parameter continuously increases from 8.192 Å to 8.219 Å with increasing the calcination temperature. According to the result of Masquelier *et al.*,[24] the calcination temperature influences strongly on the cubic lattice parameter and the real stoichiometry of spinel lithium manganite, which lies between $LiMn_2O_4$ and defect spinel $Li_2Mn_4O_9$ containing vacancies on both the lithium and the manganese sites if Li/Mn ratio is 1/2. The lattice parameters of 8.192-8.219 Å for the powder calcined at 400-700 °C are intermediate values between those reported for $LiMn_2O_4$ (a= 8.248 Å, oxidation state of Mn=3.5) and $Li_2Mn_4O_9$ (a=8.162 Å, oxidation state of Mn=4.0). The cubic lattice parameters also indicate that the average oxidation state of Mn lies between 3.5+ and 4+.

Magnetic behaviors of the calcined powders. Figure 6 shows the temperature dependence of magnetic susceptibility χ and inverse magnetic susceptibility χ^{-1} for the calcined powders. As the temperature was lowered from 300 K, χ of every powder increase monotonically down to around 150 K. In addition, the value of χ was found to decrease with increasing the calcination temperature. As seen in χ^{-1}, an approximately linear relationship between χ^{-1} and temperature was observed in the temperature range between 150 and 300 K. In this range, each plot may be represented by a straight line obeying the Curie-Weiss law $\chi^{-1}=(T-\theta)/C$. It is observed that a rather regular decrease of the Weiss constant with the calcination temperature increases (Table 2), which reflects a progressive change in the relative strengths of the antiferromagnetic and the ferromagnetic interactions between Mn^{n+} cations in these lithium manganites.[24] However, at temperatures below 150 K, χ^{-1} of every sample began to deviate from the linear relationship; that is, the slope of χ^{-1} was steeper than that above 150 K. This is due to an antiferromagnetic ordering of Mn moments at low temperatures.

Powder characteristics of spinel $LiMn_2O_4$. SEM

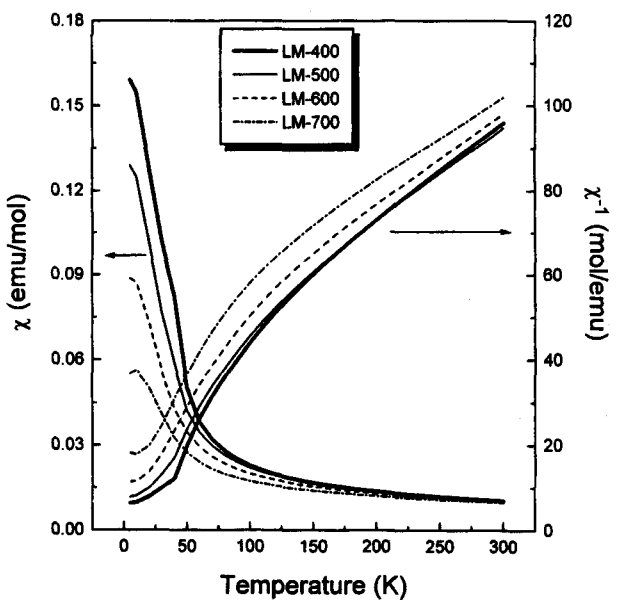

Figure 6. Molar magnetic susceptibility and inverse molar magnetic susceptibiltiy versus absolute temperature for the powder calcined powders.

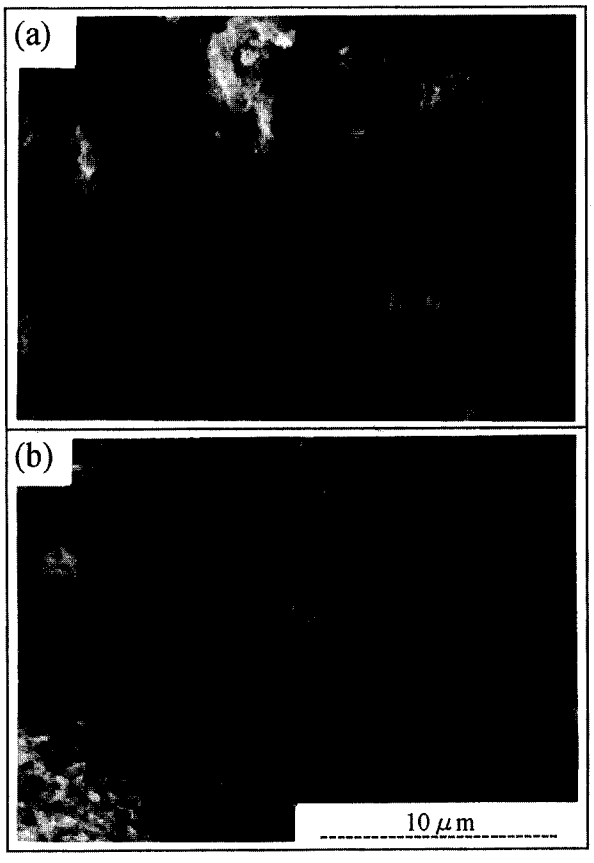

Figure 7. SEM micrographs of (a) LM-500 and (b) LM-700.

photographs of LM-500 and LM-700 are shown in Figure 7. All the powders are consisted of very fine particles, those which are highly agglomerated shape irrespective of the calcination temperature. In order to check the distribution of particle, the particle size analysis was performed by particle size analyzer as illustrated in Figure 8. The calcined powders at 400-700 °C show very broad particle size distributions, which is nearly constant irrespective of the calcination temperature. The mean diameter of the calcined powder is slightly increased with the calcination temperature. These results are in agreement with the fact that the particles are highly agglomerated as observed in SEM micrographs.

Conclusion

The citrate sol-gel method is an useful method for synthesizing spinel lithium manganite cathode material. A single phase of spinel lithium manganite could be successfully prepared by the decomposition of citrate gel at low temperature of 400 °C, *via* an intermediate state containing minor phases such as Mn_3O_4 and Li_2CO_3. The cubic lattice parameter of lithium manganite and average oxidation state of manganese strongly depends on the calcination temperature. The plot of χ^{-1} versus temperature indicates the presence of antiferromagnetic ordering of manganese at low temperature. The calcined powders were composed of submicron-sized particles, but highly agglomerated and thus showed broad particle size distribution.

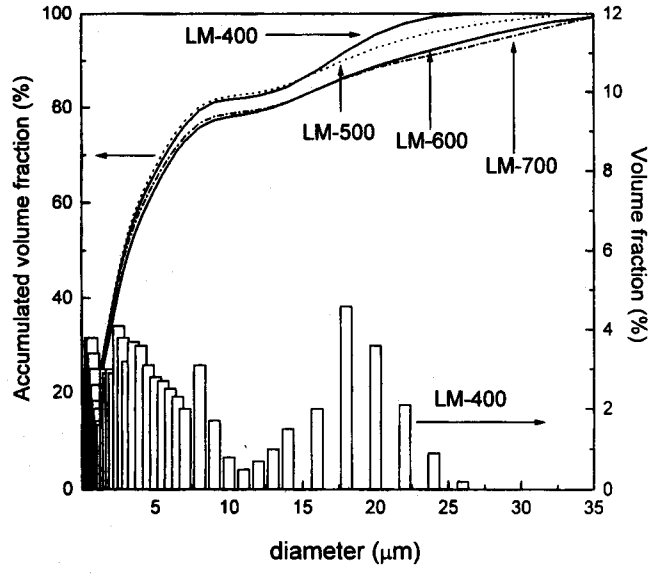

Figure 8. Volume fraction of the calcined powder and particle size distribution of LM-400 (column).

Acknowledgment. We wish to express our heartfelt appreciation to Ministry of Education for financial support (BSRI-96-3404). We are also indebted to Dr. Yang-Su Han for his comment during the experiment.

References

1. Ohzuku, T.; Kitagawa, M.; Hirai, T. *J. Electrochem. Soc.* **1990**, *137*, 769.
2. Masquelier, C.; Tabuchi, M.; Ado, K.; Kanno, R.; Kobayashi, Y.; Maki, Y.; Nakamura, O.; Goodenough, J. B. *J. Solid State Chem*, **1996**, *123*, 255.
3. Momchilov, A.; Manev, V.; Nassalevska, A. *J. Power Sources* **1993**, *41*, 305.
4. Chick, L. A; Pederson, L. R.; Maupin, G. D.; Bates, J. L.; Thomas, L. E.; Exarhos, G. *J. Mater. Lett.* **1990**, *10*, 6.
5. Shin, H.-C.; Lee, K.-R.; Park, S.; Jung, C.-H.; Kim, S.-J. *Jpn. J. Appl. Phys.* **1996**, *35*, L996.
6. Manoharan, S. S.; Paril, K. C. *J. Solid State Chem.* **1993**, *102*, 267.
7. Kingsley, J. J.; Suresh, K.; Patil, K. C. *J. Solid State Chem.* **1990**, *87*, 435.
8. Traversa, E.; Sakamoto, M.; Dadaoka, Y. *J. Am. Ceram. Soc.* **1996**, *79*, 1401.
9. Taguchi, H.; Sugita, A.; Nagao, M. *J. Solid State Chem.* **1996**, *121*, 495.
10. Park, H.-B; Kweon, H.-J.; Hong, Y.-S.; Kim, S.-J.; Kim, K. *J. Mater. Sci.* **1997**, *32*, 57.
11. Kweon, H.-J.; Kuk, S.-T.; Park, H.-B.; Park, D. G.; Kim, K. *J. Mater. Sci. Lett.* **1996**, *15*, 428.
12. Liu, W.; Farrington, G. C.; Chaput, F.; Dunn, B. *J. Electrochem. Soc.* **1996**, *143*, 879.
13. Park, H.-B.; Hong, Y.-S.; Yi, J.-E.; Kweon, H.-J. *Bull. Korean Chem. Soc.* **1997**, *18*, 612.
14. Sun, Y.-K.; Oh, I.-H. *J. Mater. Sci. Lett.* **1997**, *16*, 30.
15. Chang, S. H.; Kang, S.-G.; Jang, K. H. *Bull. Korean Chem. Soc.* **1997**, *18*, 61.

16. Harris, Daniel C. *Quantitative Chemical Analysis*; 3rd. ed., Freeman, 1991
17. Stumm, W.; Morgan, James J. *Aquatic Chemistry*; John Wiley & Sons: 1981.
18. Snoeying, V. L.; Jenkins, D. *Water Chemistry*; John Wiley & Sons: 1980.
19. Perrin, Douglas, D. *Organic Ligands*; Pergamon press: 1979.
20. Han, Y.-S. Ph. D. Thesis, Seoul National University, Korea, 1995.
21. Zhang, H.-M.; Teraoka, Y.; Yamazoe, N. *Chem. Lett.* **1987**, 665.
22. Ross, S. D. *Inorganic Infrared and Raman Spectra*; McGraw-Hill Book Company: London, U.K., 1972.
23. Wen, S. J.; Richardson, T. J.; Ma, L.; Striebel, K. A.; Ross Jr, P. N.; Cairns, E. J. *J. Electrochem. Soc.* **1996**, *143*, L136.
24. Masquelier, C.; Tabuchi, M.; Ado, K.; Kanno, R.; Kobayashi, Y.; Maki, Y.; Nakamura, O.; Goodenough, B. *J. Solid State Chem.* **1996**, *123*, 255.
25. Jang, D. H.; Shin, Y. J.; Oh, S. M. *J. Electrochem. Soc.* **1996**, *143*, 2204.

Stability Studies of Divalent and Trivalent Metal Complexes with 1,7,13-Trioxa-4,10,16-triazacyclooctadecane-N,N',N"-tri(methylacetic acid)

Choonpyo Hong*, Dong Won Kim†, and Ki-Young Choi‡

**Department of Chemical Education, Kongju National University, Kongju 314-701, Korea*
†Department of Chemistry, Chungbuk National University, Cheongju 361-763, Korea
‡Department of Chemistry, Mokwon University, Teajon 301-729, Korea
Received April 29, 1997

The potentiometric methods have been used to determined the protonation constants ($\log K_i^H$) for the synthesized 1,7,13-trioxa-4,10,16-triazacyclooctadecane-N,N',N"-tri(methylacetic acid) [N_3O_3-tri(methylacetic acid)] and the stability constants ($\log K_{ML}$) of the complexes of divalent and trivalent metal ions with the ligand N_3O_3-tri(methylacetic acid). The protonation constants of N_3O_3-tri(methylacetic acid) were 9.70 for $\log K_1^H$, 9.18 for $\log K_2^H$, 7.27 for $\log K_3^H$, *3.38 for* $\log K_4^H$, and 2.94 for $\log K_5^H$. The stability constants for the complexes of divalent metal ions with N_3O_3-tri(methylacetic acid) were 10.39 for Co^{2+}, 10.68 for Ni^{2+}, 13.45 for Cu^{2+}, and 13.00 for Zn^{2+}. The order of the stability constants for the complexes of the divalent metal ions with N_3O_3-tri (methylacetic acid) was $Co^{2+}<Ni^{2+}<Zn^{2+}<Cu^{2+}$. The stability constants for the complexes of trivalent metal ions with N_3O_3- tri(methylacetic acid) were 16.20 for Ce^{3+}, 16.40 for Eu^{3+}, 16.27 for Gd^{3+}, and 15.80 for Yb^{3+}. The results obtained in this study were compared to those obtained for similar ligands, 1,7-dioxa-4,10,13-triazacyclopetadecane-N,N',N"-tri(methylacetic acid) and 1,7,13-trioxa-4,10,16-triazacyclooctadecane-N,N',N"-triacetic acid, which have been previously reported.

Introduction

The first macrocyclic compounds containing polyether were reported by Lutteringhaus and Ziefler in 1973.[1] These macrocyclic compounds showed remarkable selectivities toward certain metal ions for the complex formation, and then such ligands can be used in the fields of biochemistry, hydrometallurgy and waste treatment.[2-7]

The objective of their research was to determine the stability constants of complexes of some divalent and trivalent metal ions with the macrocyclic ligand having methylacetate groups as N-pendant arms. The stability constants of the metal ions with macrocyclic ligands were determined by various methods. Delgado *et al.*[8] determined the stability constants of the complexes of some divalent and trivalent metal ions with a series of macrocyclic ligands having acetate groups as N-pendant arms. These series of ligands provided an opportunity to study on the influence of the steric effect of the macrocyclic ring and increasing number of donor atoms on the stability and selectivity of metal complexes. The metal ions studied include the divalent metal ions, such as Co^{2+}, Ni^{2+}, Cu^{2+}, Zn^{2+}, Ca^{2+}, and Pb^{2+}, and trivalent metal ions such as Al^{3+}, Ga^{3+}, Fe^{3+}, In^{3+}, and Gd^{3+}. The series of ligands, which are N,N',N"-triazacyclononane triacetic acid [N_3-triacetic acid],[9] 1-oxa-4,7,10-triazacyclododecane-N,N',N"-triacetic acid [N_3O-triacetic acid],[10] and 1,7-dioxa-4,10,13-triazacyclopetadecane-tri(methylacetic acid [N_3O_2-tri(methylacetic acid)],[11] also provided an opportunity to compare the affinities to the metal ions.

In this work, the protonation constants of the synthesized 1,7,13-trioxa-4,10,16-triazacyclooctadecane-N,N',N"-tri (methylacetic acid) [N_3O_3-tri(methylacetic acid)] and the stability constants of the complexes of some divalent transition metal ion (Co^{2+}, Ni^{2+}, Cu^{2+} and Zn^{2+}) and trivalent lanthanide metal ions (Ce^{3+}, Eu^{3+}, Yb^{3+} and Gd^{3+}) with this macrocyclic ligand were determined. The ligands of N_3O_2-tri (methylacetic acid) and N_3O_3-triacetic acid have been studied previously.[8,11] The results obtained in this experiments